PFC/JA-85-45

IMPURITY SOURCES DURING LOWER-HYBRID HEATING ON ALCATOR C

B. Lipschultz, B. LaBombard, H. L. Manning, J. L. Terry,
S. Knowlton, E. S. Marmar, M. Porkolab, J. Rice,
Y. Takase, S. Texter, A. Wan

Plasma Fusion Center
Massachusetts Institute of Technology
Cambridge, MA 02139

December 1985

This work was supported by the U.S. Department of Energy Contract No. DE-AC02-78ET51013. Reproduction, translation, publication, use and disposal, in whole or in part by or for the United States government is permitted.

Submitted for publication in: Nuclear Fusion

By acceptance of this article, the publisher and/or recipient acknowledges the U.S. Government's right to retain a non-exclusive, royalty-free license in and to any copyright covering this paper.

IMPURITY SOURCES DURING LOWER-HYBRID HEATING ON ALCATOR C

B. LIPSCHULTZ, B. LaBOMBARD, H. L. MANNING, J.L. TERRY,
S. KNOWLTON, E.S. MARMAR, M. PORKOLAB, J. RICE,
Y. TAKASE, S. TEXTER, A. WAN

Plasma Fusion Center
Massachusetts Institute of Technology
Cambridge, Massachusetts, U.S.A.

Abstract: Impurity source mechanisms that appear during the injection of Lower-Hybrid frequency waves to heat the Alcator C tokamak are described. Si is a dominant impurity in these experiments, where SiC was the limiter surface material. At low values of injected power, the silicon source rate is dominated by physical sputtering. As the amount of injected power is raised, evaporation becomes the primary source for impurities entering the plasma. Measurements of Si line emission from the plasma, as well as other central and edge parameters are presented as functions of injected rf power.

1. Introduction

The study of auxiliary heated, tokamak fusion plasmas has become increasingly important over the past decade in light of the technical difficulty of reaching fusion conditions with ohmic-heating alone. With the increased usage of auxiliary heating has come the realization that these tokamak plasmas often have different confinement and cleanliness characteristics in comparison to ohmically-heated plasmas. In particular, studies of radio-frequency (rf) wave heated plasmas have unveiled a host of phenomena

which are responsible for generation of impurities. In most cases, the impurity increases engendered by rf wave injection usually do not threaten the continuation of the tokamak plasma discharge. However, as larger amounts of rf power are injected and the rf injection period is lengthened, this situation may change.

At Alcator C, plasmas heated by application of rf power in the Lower-Hybrid (LH) frequency range (4.6 GHz) have been studied extensively[1]. These waves have proven to be practical both in heating electrons and in driving current in the plasma. A rise in impurity line emission will often accompany the injection of these rf waves into the tokamak. Previous work[2,3] postulated that the impurity increase was due to the evaporation of limiter material. The source of heat which raises the limiter temperature was ascribed to the energy carried by LH-heated non-thermal electrons which diffuse out of the plasma. The orbits of this high-energy electron population are shifted outward in major radius with respect to the plasma flux surfaces, thus intersecting a small area of the limiter surface, creating large heat fluxes even with little total power flow. In Alcator C this interaction would occur at the larger major radius edge of the plasma.

This paper presents experimental data and corresponding modelling of the dominant impurity generation processes active during Lower-Hybrid heating of the plasma. Evidence is presented which supports the hypothesis that evaporation is responsible for most of the increase in impurity influx at large values of injected rf powers. However, the evaporation process is not the dominant rf related impurity source mechanism at lower rf powers ($P_{rf} < 550$ kW), where it is superseded by physical sputtering due to changes in the edge thermal plasma. For a particular rf power, the dominance of either physical sputtering or evaporation as the principal impurity source process is determined by the limiter material (thermal and vapor pressure properties), limiter geometry (areas involved in the different processes), densities and temperatures in the scrape-off layer and some properties of the central plasma such as energy and density of the non-thermal electrons.

2. Experiment Description

Alcator C has major and minor radii of 64 and 16.5 cm respectively. Unless otherwise specified, the results discussed here were obtained with three pairs of poloidal limiter rings. The plasma-facing sides of these limiters consisted of graphite blocks with a thin (100 micron) coating of SiC deposited using a chemical vapor process. The typical operating parameters during this set of LH wave heating experiments were a toroidal field of 8 Tesla, plasma current of 350 kA, $\bar{n}_e \approx 1.5 \times 10^{14}$ cm^{-3} with central ion and electron temperatures during ohmic operation of 1.0 and 1.7 keV respectively. A number of diagnostics were used to determine the dominant impurity generation mechanisms. The primary instruments used in this study were a grazing-incidence spectrometer, medium-energy x-ray (5 keV $\leq h\nu \leq$ 60 keV) pulse-height analyzer and a Langmuir probe array.

A grazing-incidence spectrometer was used to quantify the density of silicon in the plasma and its source rate at the edge. Silicon and carbon were the primary elements in the limiter and also the dominant impurities generated during these rf heating experiments. The spectrometer is absolutely calibrated across the wavelength region from 50 Å to 1100 Å. It viewed the plasma along a horizontal chord at the midplane of the tokamak. The detector for this spectrometer is a microchannel plate image-intensifier, coupled to a Reticon photodiode array which allows measurement of spectra (typically 50 Å at a time) at a 0.5 kHz rate. Line emission from lithium-like silicon (Si XII) was observed which is proportional to the Si density in the plasma. In steady-state, the Si XII brightness is also proportional to the Si source rate at the edge. However, in general, the time response of plasma impurity emissions to changes in edge source rate is modified by the characteristic time needed for an impurity particle, removed from the limiter at the plasma edge, to be transported to a temperature region in the plasma where the local electron temperature is sufficient for the observed ionization state to exist. It is important to keep this in mind in the discussions which follow, where time histories of impurity emissions are used to support arguments dealing with impurity source rates at the edge.

The central chord brightness of visible-Bremsstrahlung continuum emission, which is proportional to $n_e^2 Z_{eff}/\sqrt{T_e}$ was also measured during these experiments. These data, when combined with the usual electron temperature and interferometric density measurements, can be used to determine the line-averaged Z_{eff} as a function of time.

Of equal importance to the measurement of impurity line brightnesses is the simultaneous characterization of the various particle and energy fluxes which could generate the impurities. In this regard it is useful to determine the characteristics of the non-thermal electron population in the plasma by means of medium-energy x-ray emission pulse-height analysis. X-ray emission spectra, monitored by a HgI_2 detector, are obtained in the energy range 5-60 keV as shown in Figure 1. From these spectra a rough measure of N_{tail}/N_{bulk} can be calculated assuming a two-maxwellian component plasma, with

$$\frac{N_{tail}}{\sqrt{kT_{tail}}} exp\left(\frac{E_{crossover}}{kT_{tail}}\right) = \frac{N_{bulk}}{\sqrt{kT_{bulk}}} exp\left(\frac{E_{crossover}}{kT_{bulk}}\right) \tag{1}$$

where $E_{crossover}$ is as indicated in Figure 1. The 'bulk' designation is by definition the thermal component and 'tail' corresponds to the component of higher energy. T_{bulk} and T_{tail} are derived from the two characteristic slopes evident in these data. These measurements of N_{tail} & T_{tail} allow an estimate of E_{tail} ($= N_{tail} \times T_{tail}$), the energy residing in the non-thermal electron component of the plasma. That energy is proportional to P_{tail}, the power flowing out of the plasma carried by the non-thermal electrons.

The principal edge diagnostic used in characterizing edge plasma densities and temperatures for these studies was the Densepack probe array[4]. Densepack consists of a poloidal array of 80 single Langmuir probes of which 40 were used during this set of experiments. The probe array was configured to operate roughly equal numbers of the molybdenum probes at each of three different radii (16.8, 17.2, & 17.6 cm) in the shadow of the limiter (r=16.5 cm). Operation of LH wave launchers located at the same toroidal location and at toroidal locations far from the probe array indicated that the

probe results were independent of the array location with respect to the rf waveguides. A full voltage sweep of each probe tip was accomplished every 5 ms during a discharge. Standard single Langmuir probe analysis then determines n_e, T_e and floating potential as a function of radius, poloidal angle and time. For the purposes of this study, poloidal averages were performed on the probe results at each radius. No evidence of rf-pickup was found on the Langmuir probe outputs. As shown in the next section, changes in edge parameters during the rf pulse occur over time scales that are long compared to the rapid initiation of rf power. A single spatial point gridded-energy-analyzer was also used during some of these experiments to independently measure ion and electron temperatures as functions of time.

3. Experimental Results

Signals from various central plasma diagnostics collected during an experiment utilizing Lower-Hybrid rf injection (235-335 ms.) are shown in Figure 2. In addition to a small rise in central electron temperature (not shown) there is a marked rise in both the Li-like Si (Si XII) emission and X-ray flux (5 keV< E <60 keV) as indicated by traces d and e. Poloidally averaged signals from the Densepack probes at r = 17.2 cm, are shown in Figure 3. Edge ion temperatures as measured by the gridded-energy-analyzer were typically $(2-3) \times T_e$ at all times during the experiment. Edge parameter values increase on a time scale similar to those of the central plasma (e.g. Figure 2c,d) - an energy confinement time ($\tau_E \approx$10 ms.). This implies that the rf power is being deposited in the central plasma and flowing to the edge rather than being deposited directly into the edge plasma.

The changes in central and edge parameters noted above are monotonically increasing as a function of the amount of injected Lower-Hybrid rf power. For $P_{rf} \lesssim$ 550 kW, the changes in Z_{eff} as well as emission from Li-like Si during the rf pulse are approximately linearly proportional to that rf power, as shown in Figure 4(a). The corresponding Si source rates at the limiter radius are also displayed. These source

rates are inferred from the Si brightness measurements shown using an impurity transport code[5]. The two different symbols shown in this figure correspond to two different 'time signatures' of the brightness data during the rf pulse. Figure 5 illustrates this difference in 'time signatures' for several shots with $P_{rf} \approx 500$ kW. The lowest trace is typical of the Si XII brightness data shown in Figure 4 which are designated by open circles. The brightness reaches a constant level during the rf pulse. The other two traces are indicative of the data in Figure 4 designated by solid-circles. In this regime the Si XII brightness and its corresponding source rate constantly increase during the rf pulse.

At the highest rf powers injected during this set of experiments, there is a large scatter in Si brightness changes. This is not due to experimental uncertainty, but is indicative of two different impurity generation mechanisms contributing to the Si source rate. The two different impurity source mechanisms have different 'time signatures': one where the Si source rate reaches a constant during the rf pulse; a second characterized by a monotonically increasing Si brightness and corresponding source rate. These data were extended to higher values of P_{rf} in experiments where fewer limiters of the same material were used. Be-like Si (Si XI) brightnesses were measured at that time with a 1 m. grazing-incidence spectrometer. The changes in Si XI brightness and Z_{eff} are shown in Figure 6. The dominant 'time signature' of these data is again nonlinearly increasing, similar to the solid-circle data of Figure 5. This indicates that the nonlinear trend in the solid-circle data of Figure 4 extends to higher rf powers.

The energy associated with the non-thermal electron population also scales with rf power. Figure 7 shows that the characteristic temperature of non-thermal electrons scales linearly with P_{rf}. The tail electron density, N_{tail}, is typically $10^{-3} \times N_{bulk}$, slowly increasing with rf power for $P_{rf} \geq 200$ kW. In selecting the data for this plot only a small subset of data could be used due to the strong density dependence of the tail temperature upon the bulk plasma density (N_{bulk}).

Changes in the poloidal average of edge parameters (indicated by $\langle\ \rangle_{pol}$) scale in a similar fashion to central parameters. The fractional changes of both $\langle n_e \rangle_{pol}$ and

$\langle T_e \rangle_{pol}$ increase linearly with rf power (Figure 8) similar to the open circle data of Figure 4. Data are presented in terms of fractional change to remove scatter in initial values. The percentage increases in these parameters are greater at larger minor radii, indicating a slight increase of the electron density and temperature scrape-off lengths. The marked departure from linear dependence on P_{rf}, seen in the Si brightness data of Figures 4 (solid-circles) and 6, is not observed in these data.

4. Possible Sources

There are a number of different processes that can account for the aforementioned generation of impurities from the limiter[6]: physical sputtering, chemical sputtering, arcing and evaporation of limiter/first wall material as a result of interactions with non-thermal and thermal plasma. Arcing is deemed unlikely but cannot be ruled out. It typically results in irreproducible injections of impurities which is inconsistent with the observations. More importantly, the waveguides do not include Si in their structure. Chemical sputtering is of minor importance for limiter surfaces not solely consisting of graphite[7]. The SiC coating on the limiters used in these experiments eliminates this process from consideration. Two processes remain which are discussed in more detail in the following subsections.

4.1 Evaporation

The silicon source rate at high levels of injected rf power is consistent with a model in which evaporation is the dominant generation process. This can be understood by examining the strong dependence of evaporation rate, dn/dt, on the limiter surface temperature[8], $T(t)$:

$$\frac{dn(t)}{dt} = \frac{\alpha\ 3.5 \times 10^{22}\ P(T(t))}{\sqrt{M\ T(t))}} \qquad (particles/sec), \tag{2}$$

where

α = sticking coefficient,

M = atomic weight(amu) of evaporated material,

the vapor pressure, $P(T(t))$, is described by

$$P(T(t)) = P_0 \cdot exp\left(\frac{-\Delta H_m}{kT(t)}\right) , \tag{3}$$

ΔH_m is the heat of sublimation of the evaporated material, and P_0 is a constant associated with the material in question. The relationship of surface temperature to incident heat flux, $Q(t)$, is described by

$$\frac{\partial^2 T(x,t)}{\partial x^2} - \frac{\rho C_p}{\mathcal{K}} \frac{\partial T(x,t)}{\partial t} = 0 , \tag{4}$$

with the boundary condition that

$$Q(t) = -\mathcal{K} \frac{\partial T(x,t)}{\partial x}|_{x=0} \tag{5}$$

at the front surface. The temperature at the front surface (x=0), for a constant heat flux, $Q(t) = Q_0$, is

$$T(0,t) = \frac{2 \cdot Q_0 \cdot t^{1/2}}{\sqrt{\pi \rho C_p \mathcal{K}}} . \tag{6}$$

This solution is achieved with the aid of two assumptions: over the time scale of the rf pulse ($\approx$100 ms), the heat pulse propagating through the limiter block does not penetrate through to its back surface (i.e. the limiter block is treated as an infinite solid); the thermal constants of the material are assumed to be constant as a function of T(x,t)[8]. The Si evaporation rate resulting from an assumed constant heat flux, Q_0=5

kW/cm^2, turned on at t=0, is shown in Figure 9. The slope of the evaporation rate is dependent on Q_0 and duration of the heating pulse. The magnitude of this source rate and its corresponding monotonically-increasing time behavior is qualitatively similar to the Si brightness (and thus the related source rate) and Z_{eff} data shown in Figure 10 as well as the solid-circle data of Figure 5. Note that as the rf power is increased, the slope of the experimental data also increases.

There are two possible sources of such a constant heat flux which could support the hypothesis of evaporation being the dominant source process for Si. The first is due to the deposition of non-thermal electron energy from the main plasma on a small area where their orbits intersect the limiter. Measurements show that the non-thermal emission spectrum (Figure 1) and spatial profile of the medium-x-ray emission remain relatively unchanged during the rf pulse. Thus, the energy residing in the non-thermal electron population, E_{tail}, remains constant during the rf pulse. If the non-thermal particle confinement time also remains fixed during the same period, the resultant increase in limiter heat flux would follow the waveform in Figure 2e; a constant during the rf pulse.

The magnitude of this non-thermal heat flux can be roughly estimated by comparing the slowing-down time of the fast electrons (E$\approx 30-40$ keV) on the bulk plasma ($\tau_{ee} \approx 0.5$ ms) to their diffusive energy confinement time, $\tau_{n\text{-}t}$. The energy confinement times of higher energy electrons in other tokamaks [3,9,10,11], as well as in Alcator C at lower $\overline{n}_e$ [12], have been measured to be approximately equal to that of the bulk plasma energy confinement time. Therefore, given that the energy confinement time of both higher-energy (MeV) electrons and bulk electrons is of the same order, the medium-energy electrons (30-50 keV) are assumed to be the same ($\tau_{n\text{-}t} \approx 10$ ms). Furthermore, assuming that there are no anomalous loss mechanisms, the following equation describes the division of rf input power absorbed by the non-thermal population, P_{rf}, between the power deposited in the bulk plasma, P_{bulk} (slowing-down), and the power carried by the non-thermal electrons diffusing out of the plasma, $P_{lim,n\text{-}t}$:

$$P_{rf} = P_{bulk} + P_{lim,n\text{-}t} = E_{n\text{-}t}\left(\frac{1}{\tau_{ee}} + \frac{1}{\tau_{n\text{-}t}}\right) \quad . \tag{7}$$

The power carried to the limiter by the diffusing non-thermal population, $P_{lim,n\text{-}t}$, can be solved for;

$$P_{lim,n\text{-}t} = \frac{P_{rf}}{1 + \frac{\tau_{n\text{-}t}}{\tau_{ee}}} \quad . \tag{8}$$

Due to the disparity in confinement time scales found in this equation, the following approximation can be made:

$$P_{lim,n\text{-}t} \approx \frac{\tau_{ee}}{\tau_{n\text{-}t}} P_{rf} \approx 0.05 \cdot P_{rf} \quad . \tag{9}$$

The limiter area over which this power is deposited is further assumed to be defined by the spatial limits in observed limiter damage (≈ 1 cm^2/limiter) at the outside midplane section of the limiter. Then the non-thermal limiter heat flux for $P_{rf} \approx 500$ kW can be estimated: $Q_{lim,n\text{-}t} \gtrsim 5kW/\text{cm}^2$. This is an adequate heat flux, as indicated by the example of Figure 9, to explain the Si brightness data. However, there is no direct measurement of when the limiter damage was incurred.

A second possible source of a large heat flux is the flow to the limiter of thermal energy residing in the edge plasma. If this heat flux is spread exponentially in minor radius and uniformly in poloidal angle over the limiter surfaces during the rf pulse, the largest heat flux (in minor radius) would be ≈ 500 W/cm^2. This value takes into account the limiter surface curvature with respect to the incident toroidal plasma flow. The rises in limiter temperature and Si vapor pressure corresponding to this heat flux would be insignificant. However, the question arises: are the poloidal asymmetries in edge temperature and density measured by the Densepack probe array [13] large enough to generate the inferred Si source rates ($\approx 5 \cdot 10^{19}$/sec)? Results typically show

that localized peak power flows at the limiter radius are less than 2 times the average value. These enhancements over the average heat flow are still too low to produce a local limiter temperature rise and accompanying vapor pressure increase consistent with the inferred Si source rate. Therefore Si evaporation derived from the deposition of non-thermal electron energy on a small portion of the limiter surface is the most probable mechanism to explain the Si brightness data, for large values of P_{rf}.

At lower values of injected rf power, a model in which evaporation is still the dominant Si source term is not consistent with the open circle data of Figure 4. In a typical corresponding case, shown in Figure 5 (open circles), the Si XII brightness reaches an equilibrium value during the rf pulse. The silicon source rate at the edge, and necessarily the limiter surface temperature, would also have to arrive at constant values before the emission from Si XII does. After the necessary equilibrium temperature is reached, the inferred $Q_{lim}(t)$ must decay, to first order, $\propto 1/\sqrt{t}$, to reproduce the data. Neither of the two possible heat sources discussed earlier, non-thermal electrons or thermal edge plasma exhibits this time dependence.

4.2 Physical sputtering

Physical sputtering by thermal edge plasma provides a more plausible mechanism for the Si source rate at lower values of injected rf power. The flux of impurity i from the limiter surface due to thermal ion sputtering, $\Gamma_{i,sput}$, is related to edge parameters through[6]

$$\Gamma_{i,sput} = \Gamma_{th} \cdot S(E_{ion}, M_{ion}) \tag{10}$$

where

$$\Gamma_{th} = \frac{1}{2} n_i c_s \tag{11}$$

is the flux of thermal (bulk) ions to the limiter; $S(E_{ion}, M_{ion})$ and c_s their sputtering coefficient and sound speed respectively. The energy of the incident ions, E_{ion}, is linearly proportional to the edge electron temperature, T_e. In Figure 3, which is typical of the change in edge parameters during the rf pulse, Γ_{th}, and more importantly T_e, ultimately reach equilibrium values during the rf pulse. The resultant sputtering must also reach a constant value on the same time scale.

The magnitude of $\int \Gamma_{th} dA$ and S used to calculate a Si sputtering rate, were estimated on the basis of Densepack data for these discharges to be $\approx 5 \times 10^{21}$/sec and 0.025, respectively. The resulting $\Gamma_{Si,sput} \approx 10^{20}$/sec is in the range needed to explain the Si source rates inferred from Figures 4 and 6.

Physical sputtering, although still an operative mechanism, does not dominate the impurity source rate at higher values of P_{rf} where evaporation has been shown to be consistent with the data. For $P_{rf} \gtrsim 550$ kW, the Si source rate is often constantly increasing during the rf pulse (Figure 10, or solid-circles in Figure 4). For physical sputtering by thermal ions to be the principal source of this time behavior, edge parameters must also monotonically increase: however, this is not observed.

On the other hand, physical sputtering by impurity ions (self-sputtering) could, in principle, cause a monotonically increasing Si source rate if the sputtering coefficient of Si on SiC were $\gtrsim 2$. The sputtering coefficient must be greater than 1 due to equal numbers of both Si and C atoms being released and the sputtering coefficient of C on SiC being significantly lower than for Si on SiC. To achieve such a large sputtering coefficient, a Si ion must have an incident energy of about 500 eV. Assuming $T_i \approx 3 \times T_e$ and a value of $T_e \approx 20$ eV at the limiter radius, the Si ion charge needed to attain this energy must be at least 6. The calculations discussed in the following section indicate that the average charge of Si ions returning from the plasma to be closer to 3. This low value for the Si average ionization state is due to the short mean free path for ionization of neutral silicon (2-3 mm) at the limiter radius. Most of the neutral Si influx is ionized within one mean free path of the limiter radius and immediately diffuses outward into

the limiter shadow. However, a small fraction ($\approx 10^{-3}$) of the returning ions are more highly ionized. The time required for such an impurity ion to cycle through the central plasma and reach high ionization states is long ($\approx 10-20$ ms). Thus, even if these few highly-ionized ions were to produce a self-sputtering coefficient of Si on SiC $\gtrsim 2$, the Si source rate would rise more slowly than is observed. Therefore self-sputtering does not play a dominant role in impurity generation in Alcator C plasmas. The modelling in the following section supports this conclusion.

5. Analysis and Modelling of the Measurements

The conclusions of the previous section are based on qualitative arguments involving very simple calculations and 'time signatures' of the various data. At low values of injected rf power, the Si influx rate reaches a constant value during the rf pulse. This behavior is consistent with a model of physical sputtering. However, as P_{rf} is increased, the dominant 'signature' is of a nonlinearly increasing Si source rate during the rf pulse. This corresponds to evaporation derived from the deposition of non-thermal electron energy on a small fraction of the limiter area.

A numerical model has been developed to determine quantitatively the magnitude of the impurity source rates resulting from the processes discussed above. The experimental data detailing the density and temperature time dependences of both the edge plasma and the non-thermal electron population in the central plasma are used as input. The Si evaporation rate due to the associated heat fluxes can be calculated once the time dependence of the surface temperature is known. A generalization of Equation (6) is used for this purpose:

$$T(x=0,t) = T(x=0,0) + \int_0^t Q(t')\, G(t-t')\, dt' \qquad (12)$$

This represents the convolution of the surface temperature Green's function (response to a delta-function in time heat pulse) with the time-dependent incident heat flux,

$Q(t')$. The resultant evaporation rates are evaluated using Equations (2) and (3). The particular constants needed for that evaluation can be found in a number of references [14-17].

The heat flux to the limiter surface due to the thermal edge plasma is

$$Q_{th}(r,t) = \Gamma_{th}(r,t) \cdot E_{th}(r,t) \tag{13}$$

where again, $\Gamma_{th}(r,t) = 0.5\, n_{edge}(r,t)\, c_s(r,t)$, $c_s(r,t)$ is the ion sound speed and $E_{th}(r,t)$ the total energy that an ion-electron pair carries through the sheath. The latter is calculated based on a model by Emmert[18]. The dependence of non-thermal electron heat flux on injected rf power is assumed to be the same as that of the non-thermal population temperature (Figure 7). The uncertainties associated with the calculation of evaporation source rates due to thermal edge plasma and non-thermal electrons are difficult to estimate. In particular, the uncertainty in the magnitude of the limiter heat flux due to non-thermal electrons dominates the overall uncertainty of the evaporation calculation due to the exponential nature of Equation (3). This overall uncertainty is estimated to be up to a factor of 10.

The determination of the impurity influx due to physical sputtering by the edge thermal plasma is based on Equation (10). The sputtering coefficient, $S(E_{ion}, M_{ion})$, is calculated with the use of the subroutine DSPUT[19]. The energy carried by these thermal ions is again calculated using the theory provided by Reference 18.

Generalization of Equation (10) to allow for calculation of physical sputtering due to impurity ions incident on the limiter must include consideration of the two possible 'paths' ions travel before returning to the limiter; those that enter the main plasma, and those that remain in the edge. The flux of impurity neutrals leaving the limiter surface at time t' is designated to be $\Gamma_i(r,t')$. The fraction of those impurity neutrals that reach the limiter radius, and thus can be counted as impurity source reaching the main plasma, is dependent on the mean free path for ionization and the perpendicular

distance from the point of origin to the edge of the plasma. Defining f(r) to be the fraction for neutral impurities originating at radius r, the rate at which these impurities enter the plasma (the first 'path') at time t' is then

$$\frac{dN_{i,in}(t')}{dt} = \int_{\substack{lim \\ surfaces}} \Gamma_i(r,t')\, f(r)\, 2\pi r\, dr \ . \tag{12}$$

These impurities cycle through the plasma and return to the limiter. A Green's function technique is used to determine the rate, $dN_{i,out}(t)/dt$, at which impurities diffuse back out of the plasma at time t:

$$\frac{dN_{i,out}(t)}{dt} = \int_0^t G_i(t-t')\, \frac{dN_{i,in}(t')}{dt}\, dt' \ . \tag{13}$$

$G_i(t-t')$ is obtained from an impurity transport code using typical plasma parameters and the observed impurity transport relations described in Reference 5. This impurity transport code can also be used to determine $G_{Z,i}(t-t')$, a Green's function used to determine the average ionization state of impurity i leaving the plasma at time t which entered the plasma at time t'. Using a modified version of Equation (10), the sputtering due to these 'plasma' impurities can then be determined.

The second path that an impurity can follow after leaving the limiter surface is to remain in the edge plasma. These ions return to the limiter in a time much shorter than the computational time step. Therefore, this group of impurities can be considered to enhance the local thermal sputtering by the usual equilibrium amplification factor[6,20]:

$$\frac{1}{1-S_i} \ . \tag{16}$$

S_i is the sputtering coefficient for impurity i on a limiter of the same material. The average ionization state, $< Z_i >$, of this flux of impurities returning out of the plasma,

is determined by comparing the ionization time required to reach a particular charge state, with the time it takes for the singly-ionized impurity to return to the limiter. $< Z_i >$ is typically ≤ 2 for these plasmas in the limiter shadow. In the case where there are substantial densities of more than one element in the limiter surface, Equation (16) must be generalized to account for the sputtering of the limiter element i, by impurity ion j. The sputtering coefficient for such an interaction will be designated $S_{i,j}$. Defining Γ_i^I, Γ_{th}^I to be, respectively, the flux of the ith impurity ion species and thermal plasma *to* the limiter; Γ_i^{II}, the flux of ith species of sputtered neutrals *from* the limiter, then

$$\Gamma_i^{II} = \sum_j (S_{i,j}\Gamma_j^I) + S_{i,t}\Gamma_{th}^I \ . \tag{17}$$

After many generations of this interaction, an equilibrium will be reached ($\Gamma_i^I = \Gamma_i^{II}$) as long as $S_{i,j} < 1$. Then

$$\Gamma_i - \sum_j (S_{i,j}\Gamma_j) = S_{i,t}\Gamma_{th} \tag{18}$$

where $S_{i,t}$ is the sputtering coefficient of impurity i by thermal ions and the superscripts I and II have been dropped. Equation (18) is a matrix equation of the form

$$(\underline{\underline{1}} - \underline{\underline{S}}) \cdot \underline{\Gamma} = \Gamma_{th}\underline{S}_t \tag{19}$$

which can be inverted to solve for the influxes of the individual elements, Γ_j.

The principal uncertainties associated with this calculation of the various impurity source rates due to physical sputtering include: the use of poloidally-averaged edge parameters rather than the 2-D measured values; the analysis of the probe data; and sputtering coefficients used. These independent factors yield an overall uncertainty of up to a factor of 3.5. An unknown amount of uncertainty is added in not allowing for

an enhancement of $dN_{i,in}(t')/dt$ due to an inward particle convection of impurity ions from the limiter shadow region into the main plasma.

Within the framework of the model described above, the results can now be described. Figure 11 displays the numerical model output for $P_{rf} \approx 500$ kW where the data of Figures 4 and 6 are used as input. Physical sputtering due to thermal edge ions incident on the limiter (open circles) is the dominant impurity generation process for this value of injected rf power. An incremental amount of impurity influx is due to silicon and carbon ion sputtering (solid circles). The total Si source rate due to all proceses is represented by the solid triangles.

The impurity source rate due to non-thermal electron-derived evaporation (solid squares) is not dominant at the value of injected rf power chosen for the calculation depicted in Figure 11. However, slight increases in P_{rf} strongly change the situation. By inverting Equation (6), it can be seen that the time taken to reach a particular temperature (and evaporation rate) scales as $1/Q_0^2$. Figure 12 shows the results of a calculation for a slightly higher value of injected rf power ($P_{rf} \approx 600$ kW) than for Figure 11. In this case the evaporation due to the non-thermal electron-derived heat flux dominates the impurity source rate toward the end of the rf pulse. This is similar in aspect to the waveforms of Figure 5. The large variation in the Si source rate brought about by small changes in P_{rf} corresponds to the scatter found in the data of Figure 4. For both cases shown, evaporation derived from thermal plasma heating of the limiter (open squares) is insignificant.

The results shown in Figures 11 and 12 qualitatively reflect the experimental measurements of Figure 4 but quantitative differences remain. Typically, Si source rates inferred from experimental Si brightness data are at least twice those predicted by the impurity generation model based on measurements of both edge and central plasma characteristics. This difference is well within the uncertainty of either the Si source rate inferred from the impurity transport model which uses Si brightness measurements, or the uncertainty of the impurity generation model itself.

6. Conclusions

The dominant impurity generation processes in Alcator C during the injection of Lower-Hybrid rf waves to heat the plasma are physical sputtering and evaporation of silicon and carbon from the limiter surface. In the set of experiments described, physical sputtering caused by changes in the thermal edge plasma flux to the limiter was the dominant impurity generation process for $P_{rf} \lesssim 550$ kW. For larger amounts of injected rf power, the flow to the limiter of a small fraction of the high-energy electron population, with their associated energy, led to a situation where evaporation dominated the impurity generation.

These conclusions are based on both qualitative arguments relating to 'time signatures' of the two processes, as well as a quantitative model using the experimental data. The injection of rf waves into the plasma has two principal effects which bring about the impurity generation processes discussed: first, a non-thermal electron population is created with associated heat flow to the limiter; second, the temperature and density of the edge thermal plasma are increased. Qualitatively, the most important aspect of both of these effects is that they reach a constant value during the rf pulse. But this constancy engenders quite different 'time signatures' for the consequent impurity generation mechanisms: the evaporation rate due to a constant heat flux incident on the limiter surface will exponentially increase with time; physical sputtering will assume the constant nature of the energy and flux of the incident ions. This qualitative reasoning is reinforced by a time-dependent numerical model of the effects of heat and particle fluxes incident on the limiter.

The results of this study can be applied to predicting impurity production during Lower-Hybrid heating on devices other than Alcator C. If the assumption implicit in Equation (9) holds true, namely that $\tau_{n\text{-}t} \approx \tau_E$, then the non-thermal limiter heat flux can be calculated. This also assumes some estimate of the area of intersection between the non-thermal electron orbits and the limiter surface is available. Impurity source rates can be computed from Equations (2), (3) and (6). An impurity transport code

can provide the remaining information relating impurity source rates at the edge to their densities in the plasma.

Acknowledgements

The authors would like to thank the rest of the Alcator research and support staff for their assistance in the collection of this data. In addition, thanks are extended to H.W. Moos of Johns Hopkins University for the use of the VUV spectrometer used for the Be-like Si measurements. This work was carried out under U.S. D.O.E. contract # DE-AC02-78ET51013.

References

[1] Porkolab, M., Blackwell, B., Bonoli, P., Griffin, D., Knowlton, S., et al. Phys. Rev. Letters 53 (1984) 1229.

[2] Marmar, E.S., Foord, M., LaBombard, B., Lipschultz, B., Moreno, J., et al., J. Nucl. Mater. 121 (1984) 69.

[3] Cohen, S.A., Bernabei, S., Budny, R., Chu, T.K., Colestock, P., et al., J. Nucl. Mater. 128 & 129 (1984) 280.

[4] LaBombard, B., Lipschultz, B., M.I.T. Plasma Fusion Center Report PFC/JA-85-42.

[5] Rice, J.E., Marmar, E.S., Lipschultz, B., Terry, J.L., Nucl. Fusion 24 (1984) 889.

[6] McCracken, G.M., Stott, P.E., Nucl. Fusion, 19 (1979) 889.

[7] Roth, J., Bohdansky, J. & Roberto, J.B., J. Nucl. Mater., 128 & 129 (1984) 534.

[8] Behrisch, R., J. Nucl. Mater. 93 & 94 (1980) 498.

[9] Zweben, S.J., Swain, D.W. & Fleischman, H.H., Nucl. Fusion, 18 (1978) 1679.

[10] Hutchinson, I.H. & Morton, A.H., Nucl. Fusion, 16 (1976) 447.

[11] Strachan, J.D., ibid., 743.

[12] Texter, S., M.I.T. Plasma Fusion Center Report PFC/RR-85-24.

[13] LaBombard, B., Lipschultz, B., M.I.T. Plasma Fusion Center Report PFC/JA-85-43.

[14] Toulokian, Y.S., Ed., *Thermophysical Properties of High Temperature Solid Materials* (MacMillan, New York, 1970).

[15] Hultgren, R., Orr, R.L., Anderson, P.D. & Kelley, K.K., *Selected Values of Thermodynamic Properties of Metals and Alloys* (Wiley, 1963 & 1972).

[16] Honig, R.E. and Cramer, D.A., R.C.A. Review 30 (1969) 285.

[17] Drowat, J., DeMarcia, G. & Inghram. M.G., J. of Chem. Phys., 29 (1958) 1015.

[18] Emmert, G.A., Wieland, R.M., Mense, A.T., & Davidson, J.N., Phys. Fluids, 23 (1980) 803.

[19] Smith, D.L., Brooks, J.N., Post, D.E., Heifetz, D.B., in Engineering Problems of Fusion Research (Proc. 9th Symp. Chicago, 1981).

[20] Lipschultz, B., LaBombard, B., Marmar, E.S., Pickrell, M.M., Rice, J., J. Nucl. Mater.,, 128 & 129 (1984) 555.

Figure Captions

Figure 1: Typical spectrum from pulse-height-analysis of medium-energy x-rays.

Figure 2: Signals from various plasma diagnostics: a) Plasma current ($\approx 500kA$), b) $\bar{n}_e$ ($\approx 1.5 \cdot 10^{14}$cm^{-3}), c) soft-x-rays, d) Li-like Si brightness (520 Å), e) medium-x-rays (5 keV $\leq h\nu \leq$ 60 keV) and f) rf pulse; $P_{rf} = 300kW$.

Figure 3: Poloidally averaged signals from Densepack probe array at $r = 17.2$ cm

Figure 4: Changes in Li-like Si brightness (520 Å) and Z_{eff} vs. injected rf power. Si source rates are inferred from impurity transport code. Open and solid circles refer to the different 'time signatures' evidenced by data in Figure 5: solid circles - monotonic increase during rf pulse; Open circles - reach a constant value during rf pulse.

Figure 5: Li-like Si brightness (520 Å) for several shots with $P_{rf} \approx 500$ kW. Solid and open circle data correspond to same in Figure 4. Si source rates are inferred from impurity transport code.

Figure 6: Changes in Be-like Si brightness (303 Å) and Z_{eff} vs. injected rf power for earlier set of data.

Figure 7: Characteristic temperature of non-thermal electron population vs. injected rf power.

Figure 8: Poloidal average of edge parameter changes at $r = 16.8$, 17.2 & 17.6 cm, vs. injected rf power.

Figure 9: Si evaporation rate for $Q_0 = 5kW/\text{cm}^2$ heat flux incident on a SiC-coated graphite limiter. Q_0 turned on at t=0.

Figure 10: Be-like Si brightness (303 Å) and Z_{eff} vs. time for several values of injected rf power.

Figure 11: Time dependent predictions by numerical model of Si source rate vs. time during the rf pulse ($\approx$ 500 kW): Open circles correspond to the source rate

due to thermal plasma-derived physical sputtering. The incremental effect of impurity ion-derived sputtering by Si and C is indicated by solid circles. Solid squares correspond to the evaporation source rate derived from the non-thermal electron heat flux. Total source rate including impurity sputtering is given by the solid triangles. Thermal plasma-derived evaporation is negligable (open squares).

Figure 12: Same as Figure 11, but for higher value of rf power ($\approx$ 600 kW).

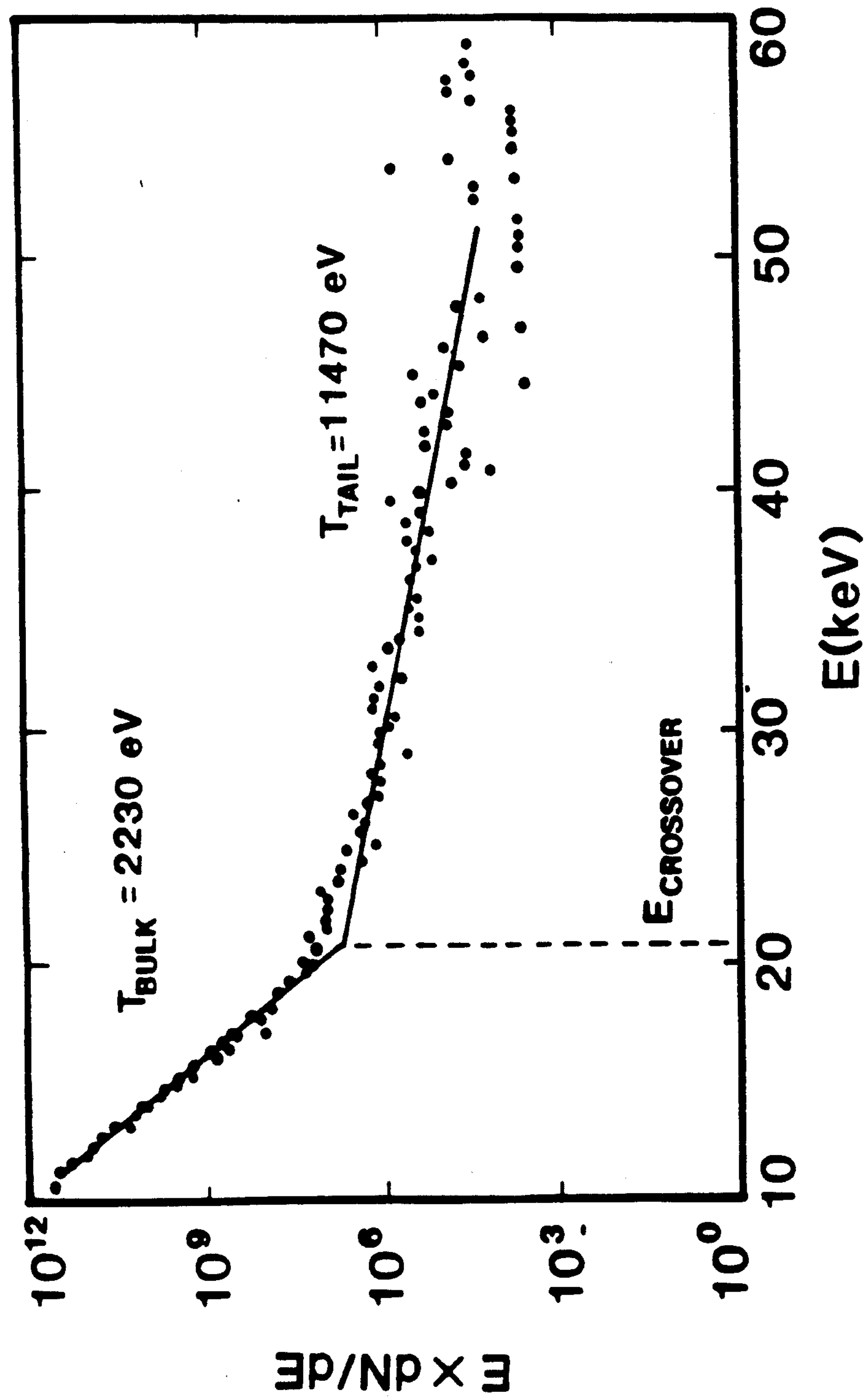

FIGURE 1

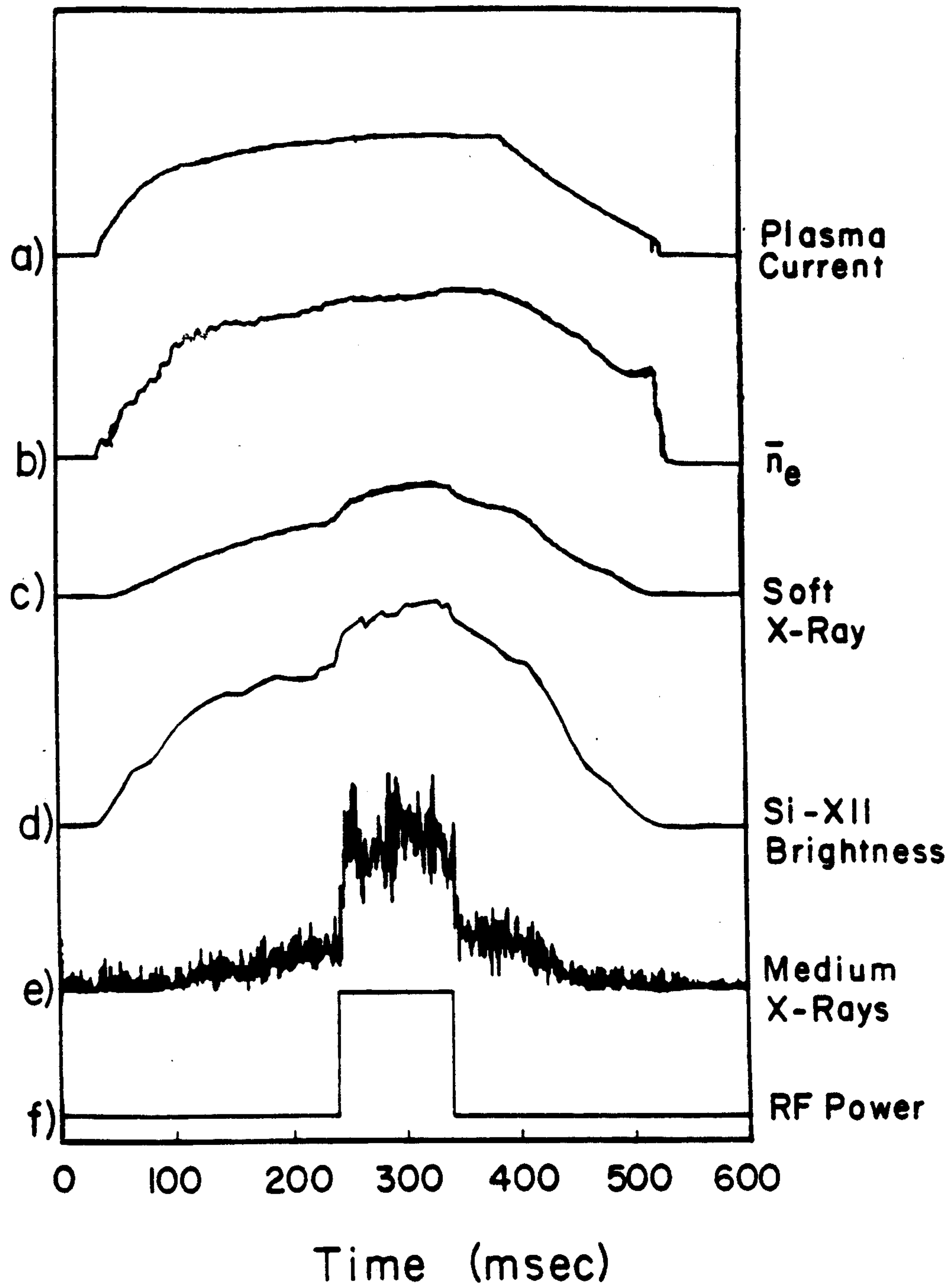

FIGURE 2

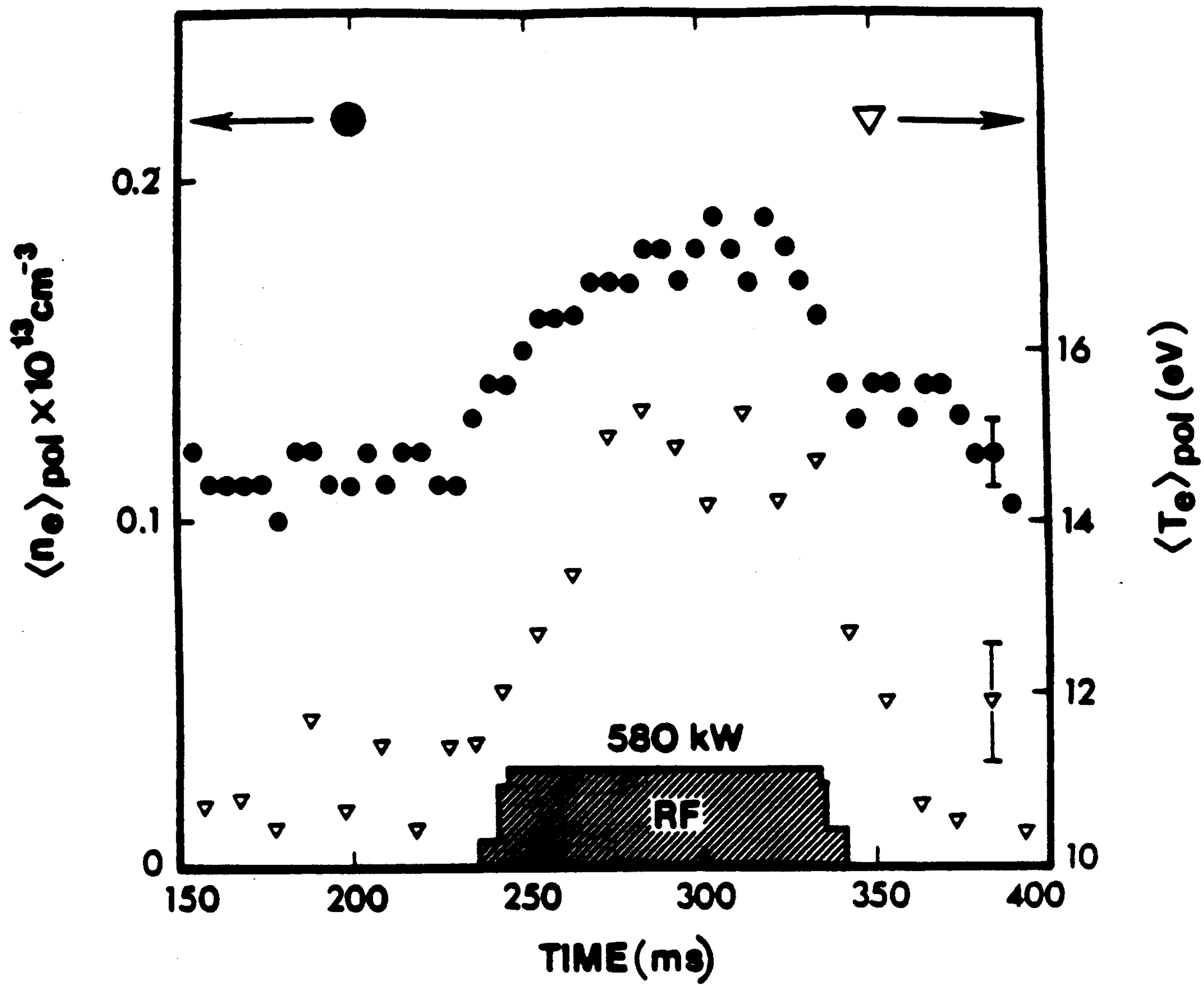

FIGURE 3

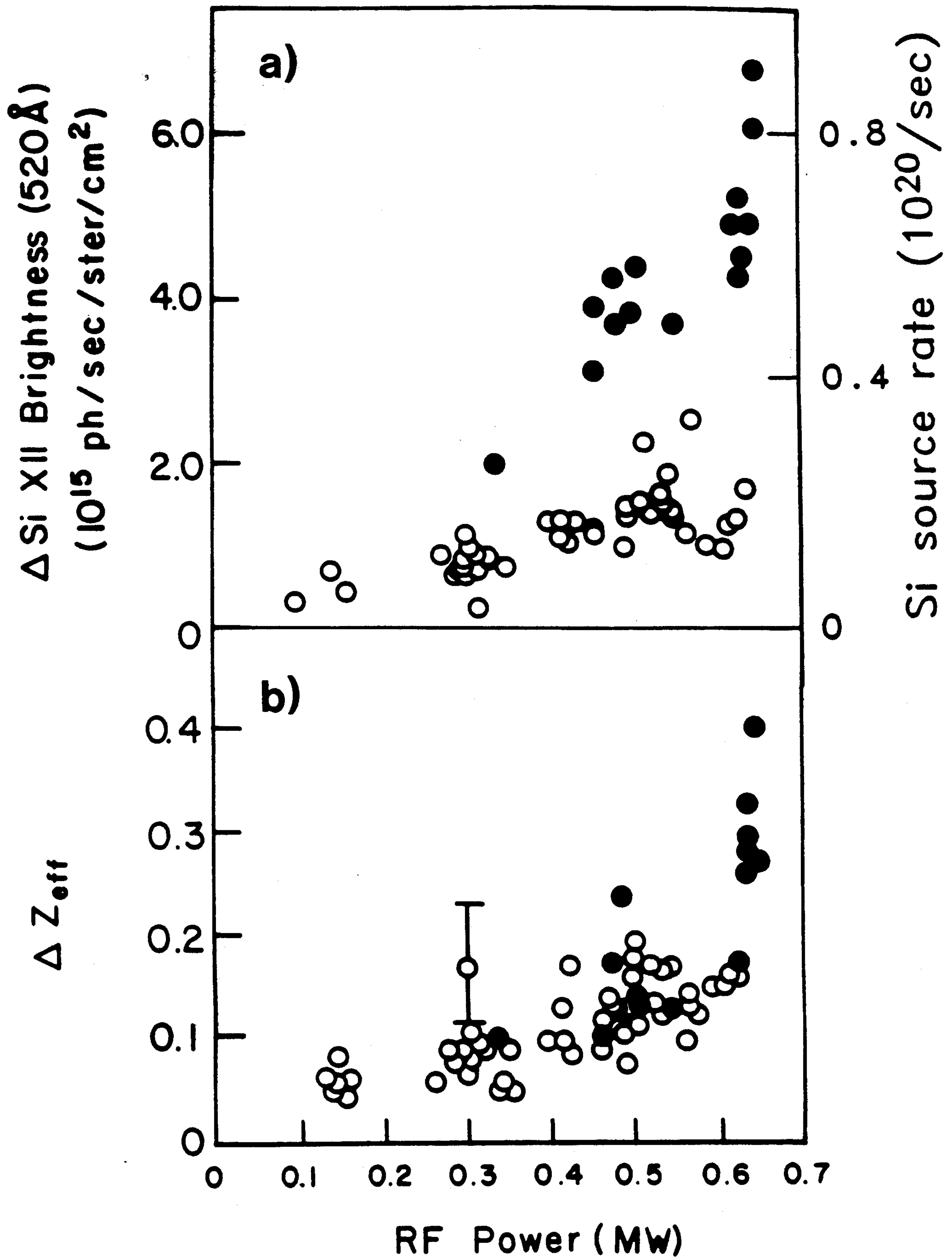

FIGURE 4

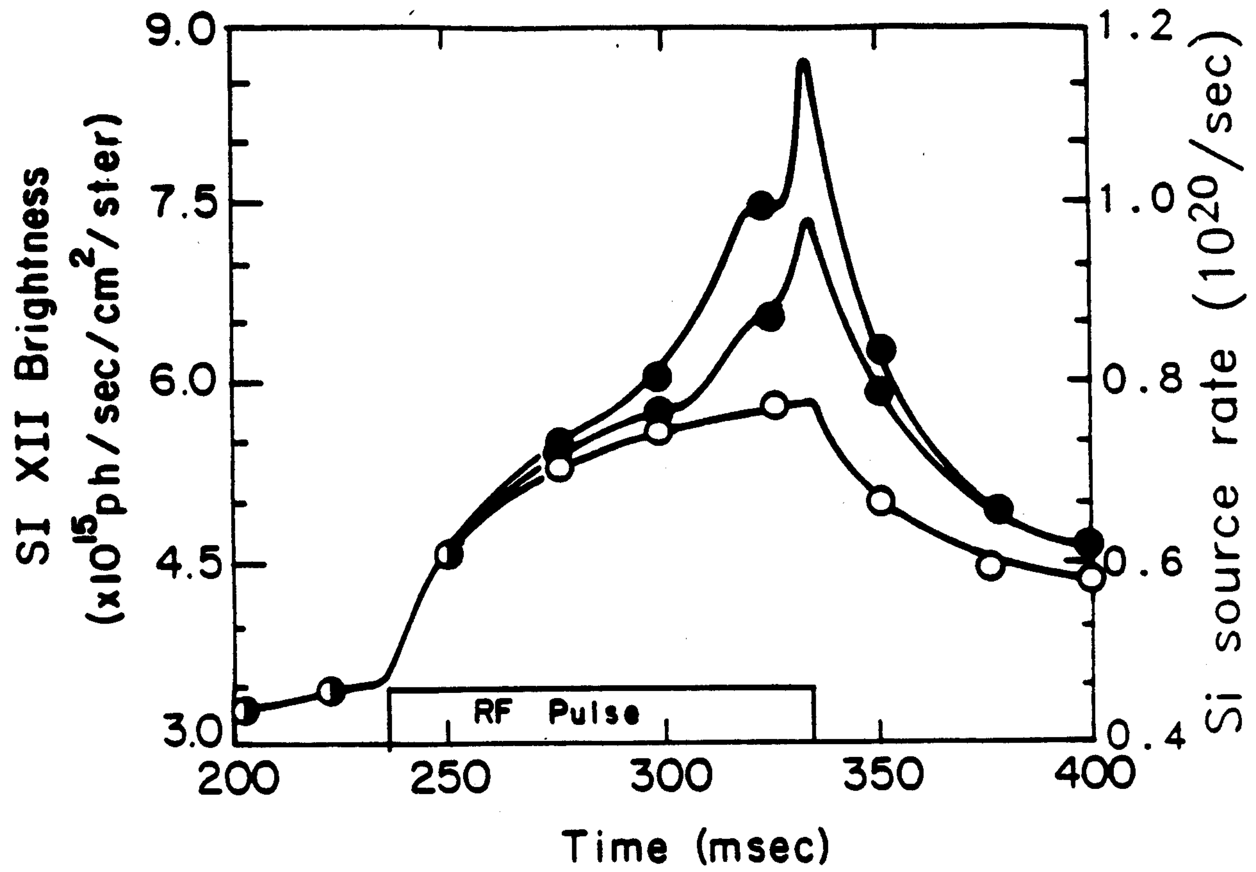

FIGURE 5

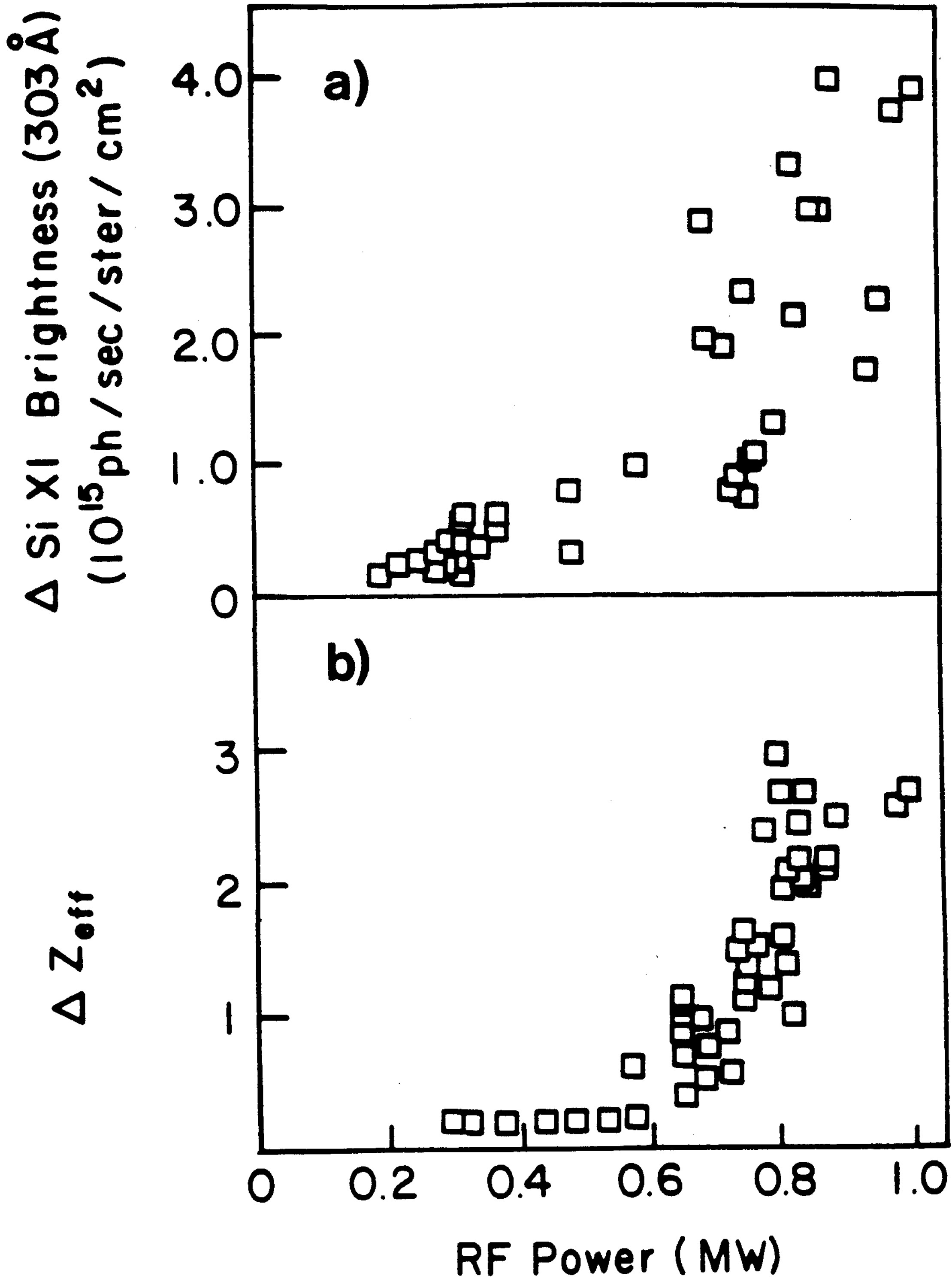

FIGURE 6

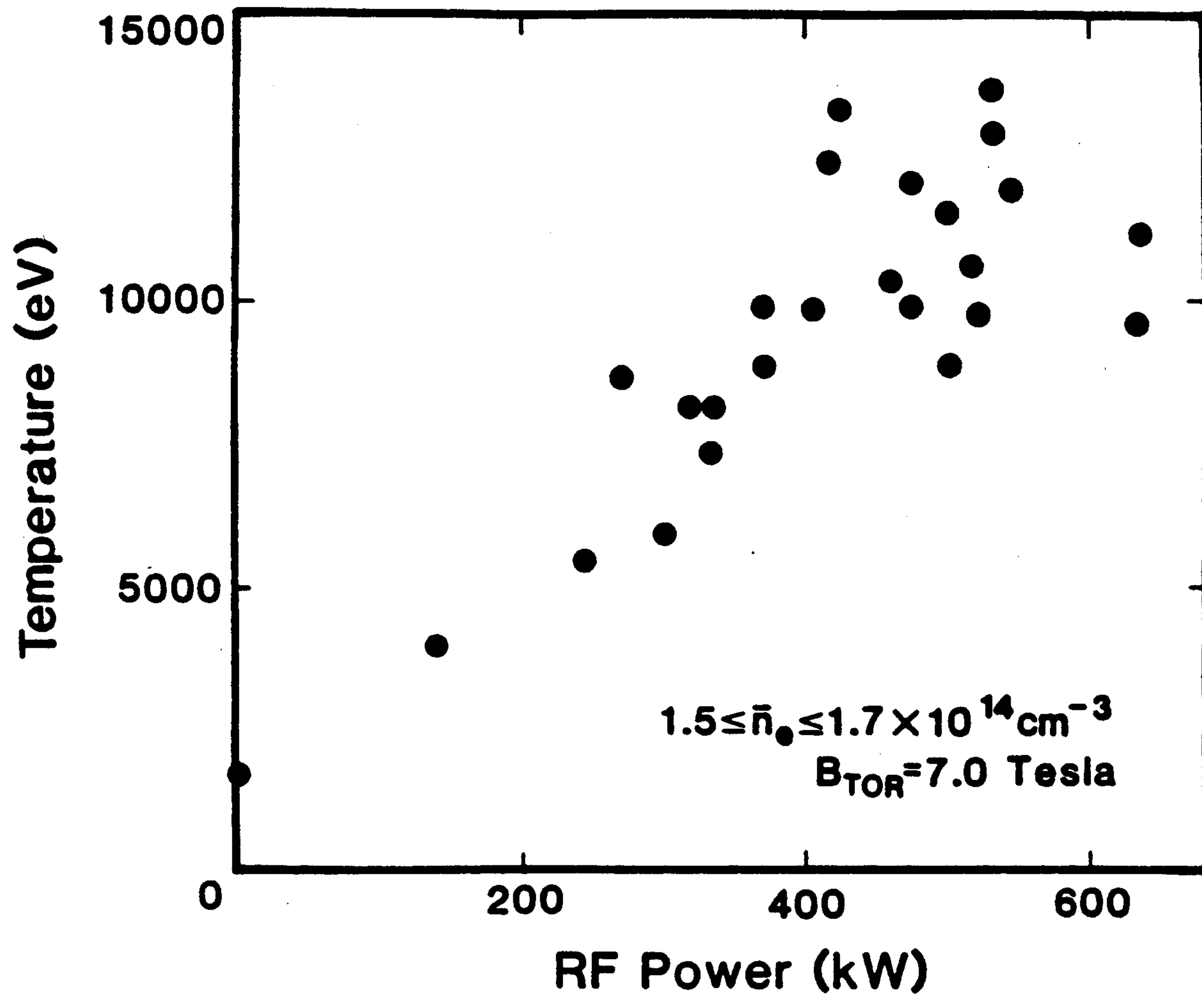

FIGURE 7

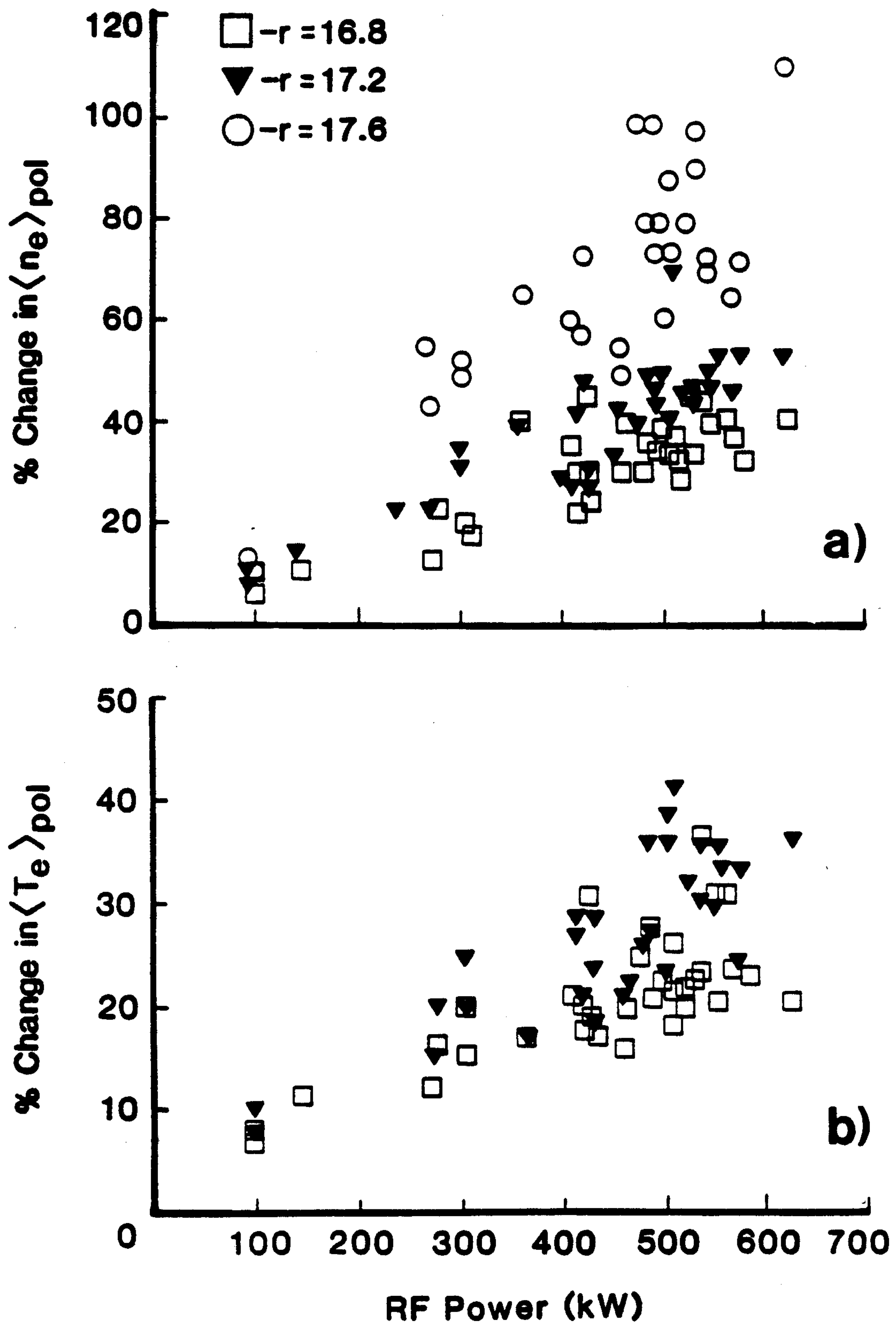

FIGURE 8

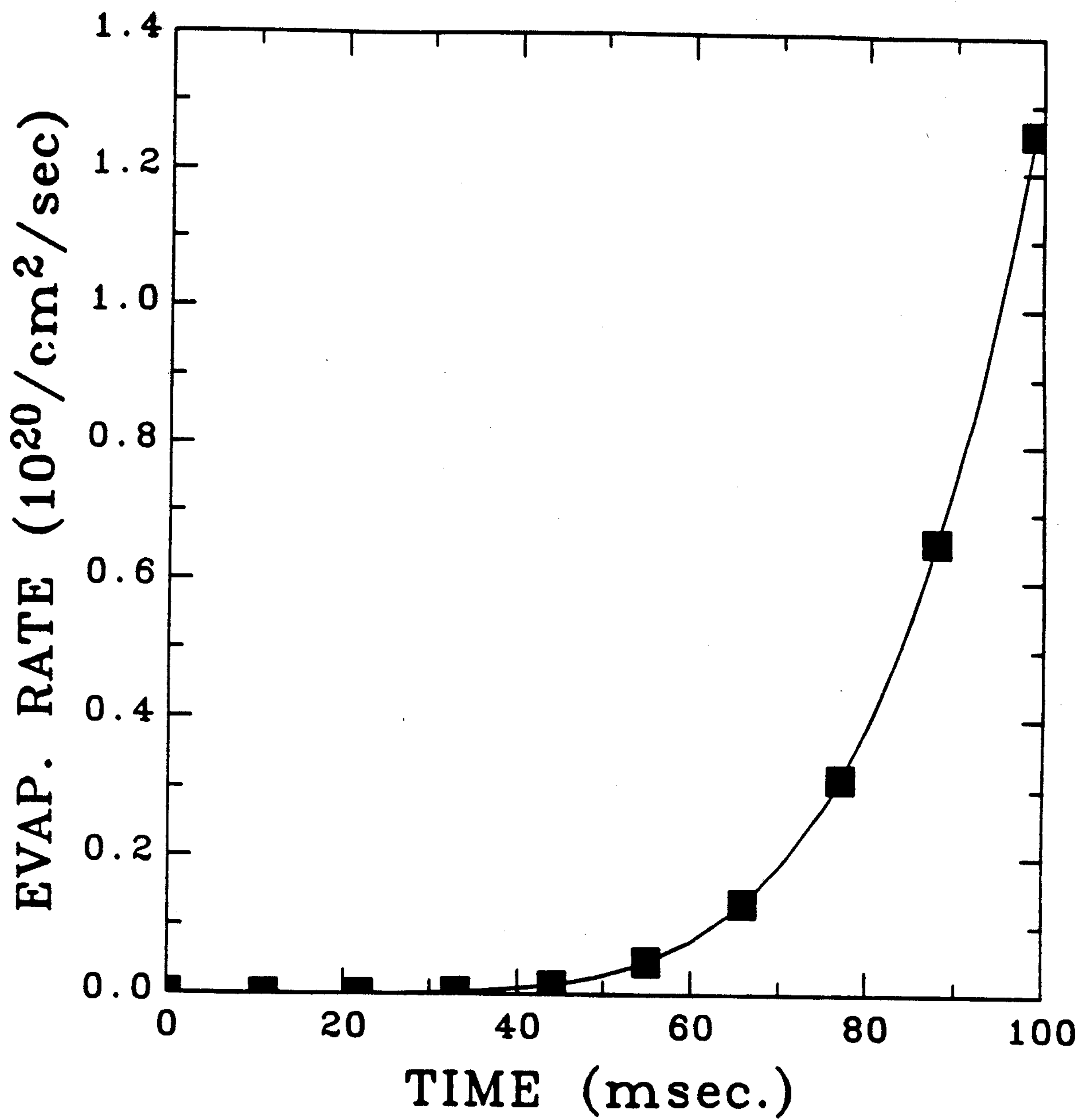

FIGURE 9

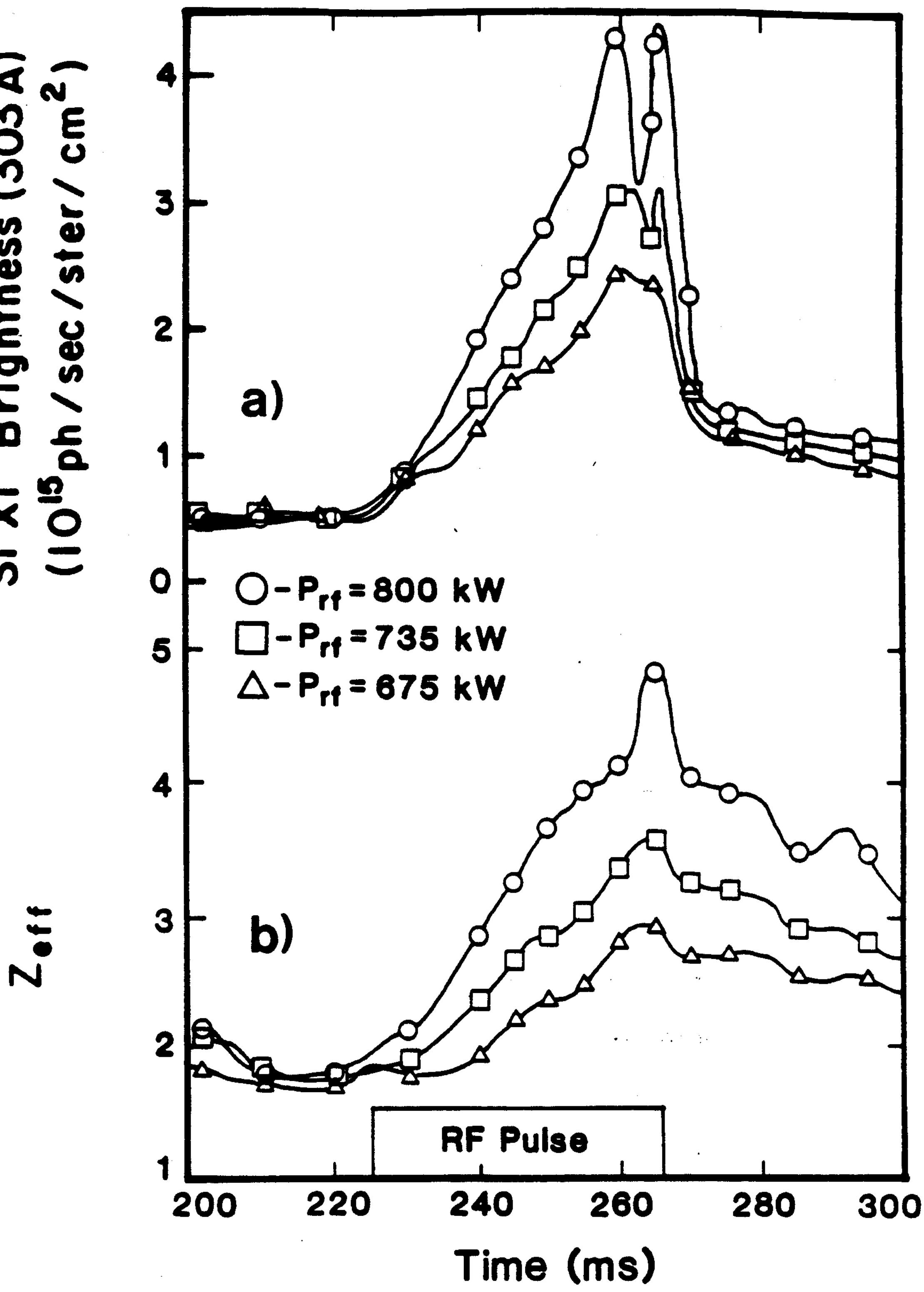

FIGURE 10

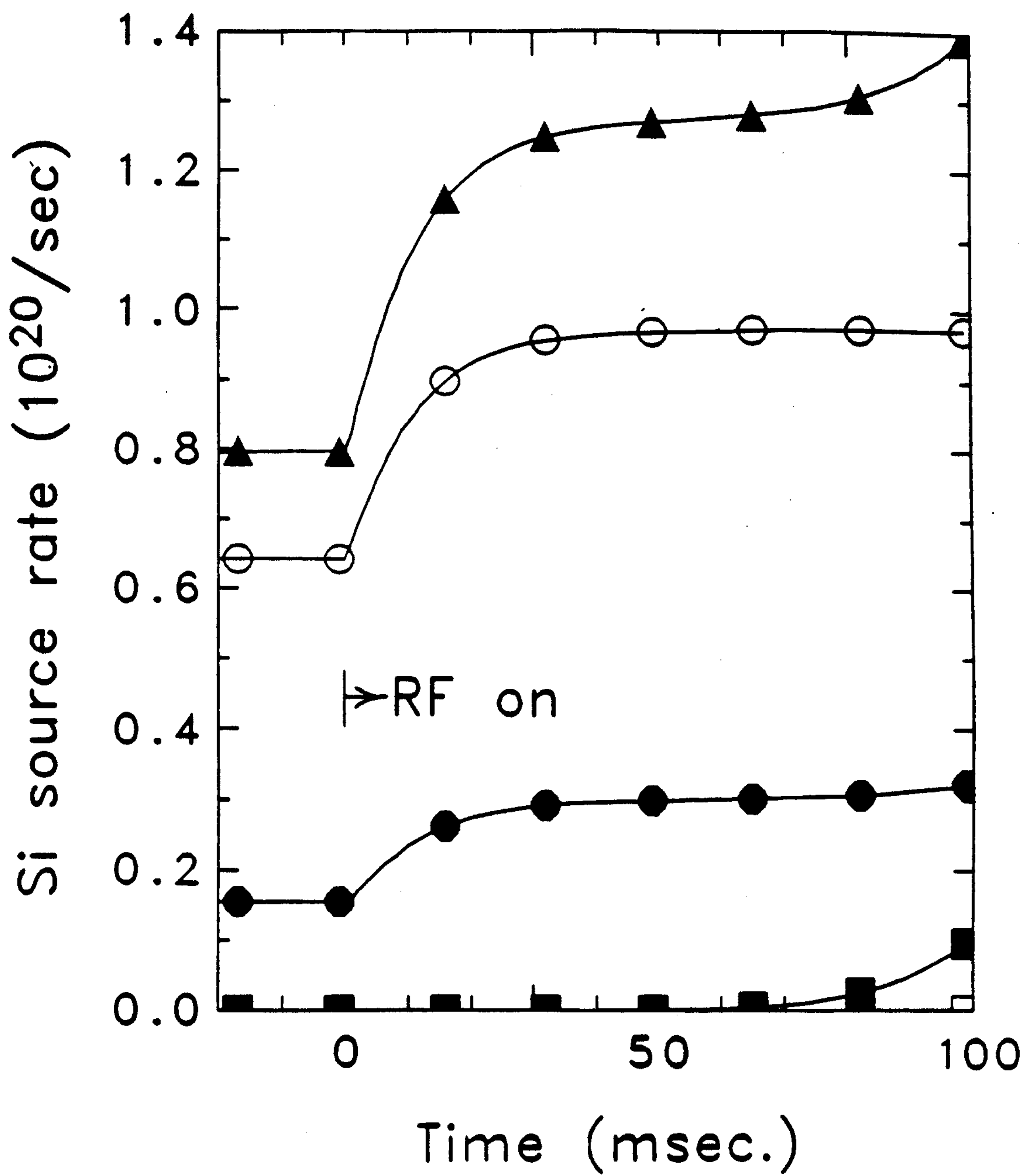

FIGURE 11

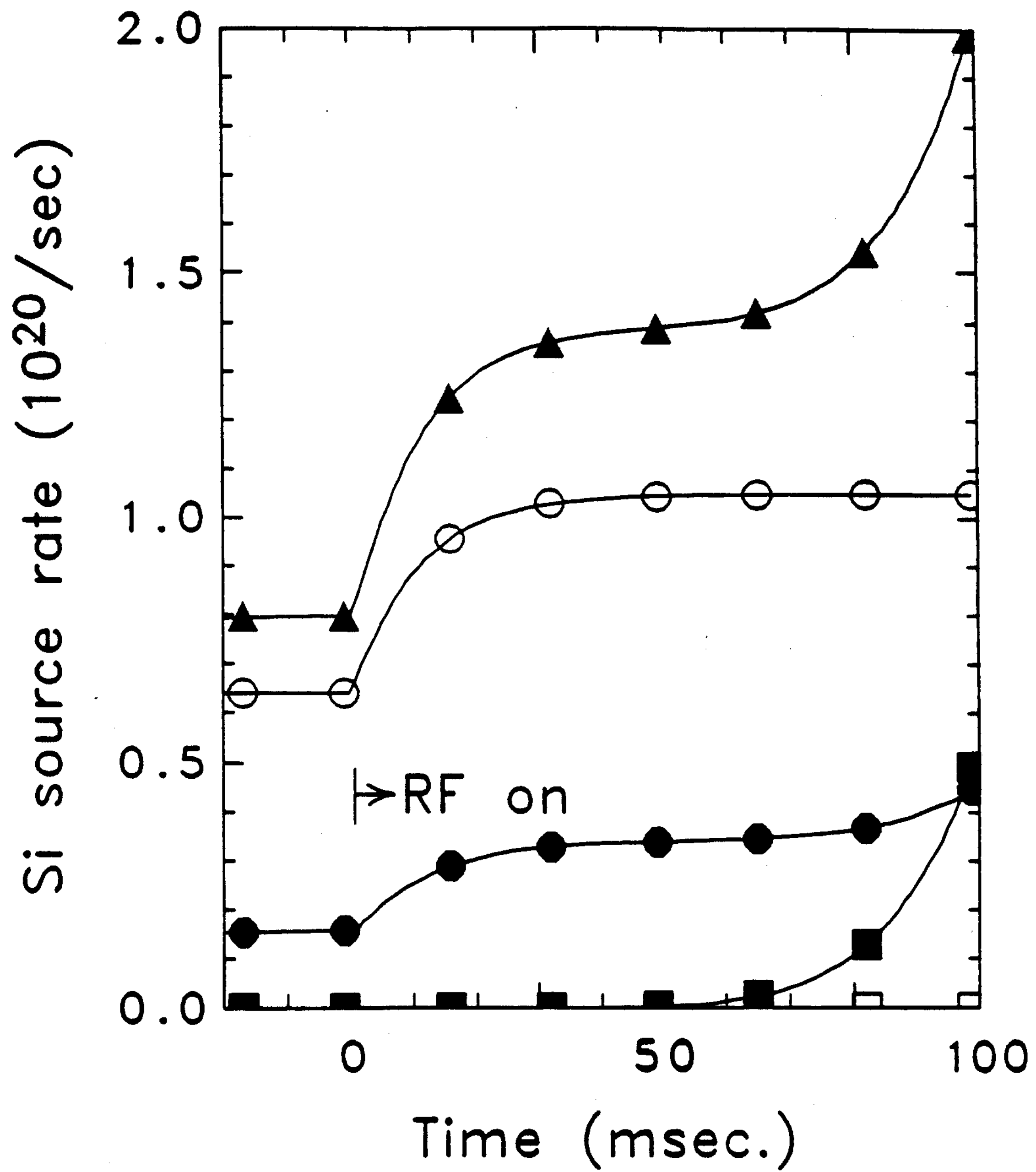

FIGURE 12